Bond electronic polarization induced by spin

Chenglong Jia,[1] Shigeki Onoda,[2] Naoto Nagaosa,[2,3,4] and Jung Hoon Han[1,5,*]

[1]*Department of Physics and Institute for Basic Science Research, Sungkyunkwan University, Suwon 440-746, Korea*

[2]*Spin Superstructure Project, ERATO, Japan Science and Technology Agency, c/o Department of Applied Physics, University of Tokyo, Tokyo 113-8656, Japan*

[3]*CREST, Department of Applied Physics, University of Tokyo, Tokyo 113-8656, Japan*

[4]*Correlated Electron Research Center, National Institute of Advanced Industrial Science and Technology, Tsukuba, Ibaraki 305-8562, Japan*

[5]*CSCMR, Seoul National University, Seoul 151-747, Korea*

(Received 17 August 2006; revised manuscript received 9 October 2006; published 29 December 2006)

We study theoretically the electric polarization induced by noncollinear spin configurations in the limit of strong Hund coupling. We employ a model of two magnetic ions sandwiching an oxygen ion. It is shown that there appears a longitudinal polarization P_x along the bond, which is roughly proportional to $(m_r^x)^2-(m_l^x)^2$ where $m_{r(l)}^x$ is the x component of the spin orientation vector at right (left) magnetic ion. A numerical study of the model Hamiltonian yields both longitudinal and transverse electric dipole moments. The transverse polarization is shown to have a nonuniform as well as a uniform component, with the latter being consistent with the previous theory. The longitudinal polarization is nonuniform and oscillating with the period half that of the spin order, but the local magnitude is typically much larger than the uniform transverse polarization and may be detected by x-ray/neutron scattering experiments.

DOI: 10.1103/PhysRevB.74.224444 PACS number(s): 75.80.+q, 71.70.Ej, 77.80.−e

I. INTRODUCTION

A number of recent experimental breakthroughs have revived interest in the phenomena of coupling of magnetic and electric (dipolar) degrees of freedom in a class of materials known as "multiferroics."[1–7] Some noteworthy observations include the development of dipole moments accompanying the collinear-to-helical spin ordering[3,4,6,7] and adiabatic control of dipole moments through sweeping of applied magnetic fields,[1,2] which all unambiguously point to the strong coupling of electric and magnetic degrees of freedom in these compounds. A number of phenomenological[8,9] and microscopic[10,11] theories has been advanced to establish the connection between noncollinear spin order and ferroelectricity.

In particular, the work of Katsura, Nagaosa, and Balatsky (KNB) (Ref. 10) proposed a microscopic theory for the interplay between noncollinear magnetic order and the dipolar polarization of the electronic wave function induced by it. The magnetic (M) ion is modeled by three degenerate t_{2g} levels experiencing some external magnetic field (to guarantee magnetic order) and subject to spin-orbit coupling. Two such magnetic ions are bridged by an intermediate oxygen (O) atom which itself has no spin-orbit interaction. Solving the model Hamiltonian perturbatively in the M-O hybridization amplitude, KNB finds an electronic polarization orthogonal to the M-O-M axis in the ground states of one and two holes.

In this paper, we revisit the M-O-M cluster model of KNB, but in the different limit of a strong Hund coupling. The M-O-M model in this limit is exactly solvable in the absence of spin-orbit coupling, with two classes of degenerate eigenstates. For these states there is no net electric polarization. The spin-orbit coupling on the magnetic sites is then introduced as a perturbation within each degenerate manifold. The problem is exactly solvable again and we can calculate the polarization $\langle \mathbf{r} \rangle$ for each of the eigenstates thus obtained. It is shown that *a nonzero polarization develops along the direction of the M-O-M cluster*. We denote such polarization as "longitudinal," to distinguish it from the "transverse" polarization, perpendicular to the cluster axis, obtained in previous theories.[8,10,11]

Numerical study of the mean-field Hamiltonian for the cluster confirms the existence of longitudinal polarization predicted analytically and reveals a nonuniform component in the transverse polarization which was unexpected in previous theories.[8,10,11] Namely, oscillating components appear in both the longitudinal and transverse polarizations with a vanishing macroscopic average whereas the polarization predicted by existing theories gives a "uniform" component induced by a noncollinear spin order.

This paper is organized as follows. In Sec. II, we introduce the mean-field Hamiltonian for the three-site cluster and, in the limit of a large Hund coupling, its approximate eigenstates are derived analytically in a perturbation theory with respect to the spin-orbit interaction. Electronic polarization is then calculated for these eigenstates to the lowest order in the spin-orbit coupling. In Sec. III, numerical solution of the mean-field Hamiltonian is presented. Fourier analysis of the polarization reveals the existence of both uniform and nonuniform components in the transverse part and a nonuniform component in the longitudinal part. We conclude with a discussion in Sec. IV. Some technical details of the derivations used in Sec. II are described in the Appendix.

II. MODEL AND ANALYTIC RESULTS

As a minimal unit giving rise to spin-polarization coupling KNB introduced the model shown in Fig. 1. To guarantee that a net average magnetic moment exists, each magnetic site is subject to a spin polarization field,[10]

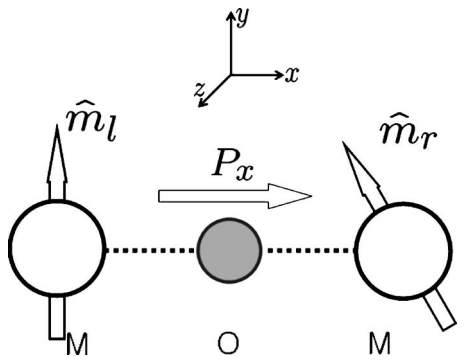

FIG. 1. Arrangement of two magnetic ions and an oxygen ion in the M-O-M cluster. $\hat{m}_l$ and $\hat{m}_r$ are the magnetic moment orientations of the magnetic sites bridged to the intervening oxygen ion. Polarization P_x along the cluster's axis is found (see text for details).

$$H_M = -U\sum_{a=l,r}\hat{m}_a\cdot\left(\sum_{b=xy,yz,zx}\mathbf{S}_{a,b}\right), \tag{1}$$

where $a=l,r$ refers to the left and right magnetic site in the M-O-M cluster as depicted in Fig. 1. Spin-orbit coupling is assumed to exist for the magnetic ions which are connected to the oxygen through the wave function overlap. The spins $\mathbf{S}_{a,b}$ in each of the three degenerate t_{2g} orbitals are subject to the local magnetic field along $\hat{m}_a=(\sin\theta_a\cos\phi_a, \sin\theta_a\sin\phi_a, \cos\theta_a)$. Ultimately such effective fields arise due to interatomic exchange interaction but also due to the strong Hund coupling within the individual magnetic ion. In such a case the strength of U mimicking the Hund coupling energy may well exceed the spin-orbit interaction strength λ. The large-U limit thus provides a natural starting point for the analysis of the spin-polarization coupling in the cluster model. In this section we propose a method that is particularly suited to treat the large U limit, namely $U\gg\lambda, V$ where V represents the M-O hybridization.

The overall Hamiltonian describing the three-atom cluster is given by $H=H_{\mathrm{M}}+H_{\mathrm{O}}+H_V$: H_{M} is already given in Eq. (1) and the other two terms, referring to the oxygen orbital and the M-O hybridization, are

$$H_{\mathrm{O}} = E_p\sum_{b=x,y,z}\sum_{\sigma}p^{+}_{b\sigma}p_{b\sigma},$$

$$H_V = V\sum_{\sigma}(d^{+}_{l,xy\sigma}p_{y\sigma}+d^{+}_{l,zx\sigma}p_{z\sigma}-d^{+}_{r,xy\sigma}p_{y\sigma}-d^{+}_{r,zx\sigma}p_{z\sigma}+\mathrm{H.c.}). \tag{2}$$

Particle-hole transformations have been implemented on all three atomic sites.[10] The on-site energy of the oxygen atom, $-E_p$, becomes $+E_p$ after the transformation. The spin-orbit interaction, not included here, will be introduced later as a perturbation.

Now we discuss how one obtains a low-energy effective Hamiltonian from Eq. (2). First, due to the large energy difference $2U$ separating the spin-up (parallel to $\hat{m}_a$) and spin-down (antiparallel to $\hat{m}_a$) t_{2g} states, we can truncate the high-energy d-orbital states from the outset and write down the effective Hamiltonian using only the low-energy operators

$$d^{+}_{a,xy} = \cos\frac{\theta_a}{2}d^{+}_{a,xy\uparrow}+e^{-i\phi_a}\sin\frac{\theta_a}{2}d^{+}_{a,xy\downarrow},$$

$$d^{+}_{a,zx} = \cos\frac{\theta_a}{2}d^{+}_{a,zx\uparrow}+e^{-i\phi_a}\sin\frac{\theta_a}{2}d^{+}_{a,zx\downarrow}. \tag{3}$$

The d_{yz} orbital does not hybridize with any of the oxygen p orbitals in the linear geometry we consider in this paper. This, and the p_x orbital which does not hybridize with any of the d orbitals, will be left out.

In this reduced Hilbert space the low-energy effective Hamiltonian becomes

$$H' = H'_{\mathrm{M}}+H'_{\mathrm{O}}+H'_V,$$

$$H'_{\mathrm{M}} = -U\sum_{a=l,r}(d^{+}_{a,xy}d_{a,xy}+d^{+}_{a,zx}d_{a,zx}),$$

$$H'_{\mathrm{O}} = E_p\sum_{\sigma}(p^{+}_{y\sigma}p_{y\sigma}+p^{+}_{z\sigma}p_{z\sigma}),$$

$$H'_V = V(d^{+}_{l,xy}p_{l,y}+d^{+}_{l,zx}p_{l,z}-d^{+}_{r,xy}p_{r,y}-d^{+}_{r,zx}p_{r,z}+\mathrm{H.c.}). \tag{4}$$

In writing down H'_V, spin rotations similar to Eq. (3) have been employed also for the p-orbital operators:

$$p^{+}_{a,y} = \cos\frac{\theta_a}{2}p^{+}_{y\uparrow}+e^{-i\phi_a}\sin\frac{\theta_a}{2}p^{+}_{y\downarrow},$$

$$p^{+}_{a,z} = \cos\frac{\theta_a}{2}p^{+}_{z\uparrow}+e^{-i\phi_a}\sin\frac{\theta_a}{2}p^{+}_{z\downarrow}. \tag{5}$$

The axis of the three-atom cluster is taken as the $+\hat{x}$ axis going from left to right in Fig. 1. Until the spin-orbit coupling is introduced, the (d_{xy},p_y) orbital pair remains decoupled from (d_{zx},p_z).

The p-orbital operators $(p_{l,y},p_{r,y})$ are not orthogonal to each other. The same is true of $(p_{l,z},p_{r,z})$. For further manipulation of the Hamiltonian we need to introduce a set of orthogonal operators

$$Y^{+}_1 = \frac{1}{\sqrt{2(1+|\kappa|)}}(p^{+}_{r,y}+e^{i\eta}p^{+}_{l,y}),$$

$$Y^{+}_2 = \frac{1}{\sqrt{2(1-|\kappa|)}}(p^{+}_{r,y}-e^{i\eta}p^{+}_{l,y}),$$

$$Z^{+}_1 = \frac{1}{\sqrt{2(1+|\kappa|)}}(p^{+}_{r,z}+e^{i\eta}p^{+}_{l,z}),$$

$$Z^{+}_2 = \frac{1}{\sqrt{2(1-|\kappa|)}}(p^{+}_{r,z}-e^{i\eta}p^{+}_{l,z}), \tag{6}$$

for the p orbitals and

$$D^+_{1,xy} = \frac{1}{\sqrt{2}}(-d^+_{r,xy} + e^{i\eta}d^+_{l,xy}),$$

$$D^+_{2,xy} = \frac{1}{\sqrt{2}}(-d^+_{r,xy} - e^{i\eta}d^+_{l,xy}),$$

$$D^+_{1,zx} = \frac{1}{\sqrt{2}}(-d^+_{r,zx} + e^{i\eta}d^+_{l,zx}),$$

$$D^+_{2,zx} = \frac{1}{\sqrt{2}}(-d^+_{r,zx} - e^{i\eta}d^+_{l,zx}), \tag{7}$$

for d-orbital states. We have defined $e^{i\eta}=\kappa/|\kappa|$, where

$$\kappa = \langle p_{l,y}|p_{r,y}\rangle = \langle p_{l,z}|p_{r,z}\rangle = \cos\frac{\theta_l}{2}\cos\frac{\theta_r}{2} + e^{i(\phi_l-\phi_r)}\sin\frac{\theta_l}{2}\sin\frac{\theta_r}{2}. \tag{8}$$

Using these new operators, the Hamiltonian in Eq. (4) becomes

$$H = H_Y + H_Z,$$

$$H_Y = -\sum_{\alpha=1,2}(D^+_{\alpha,xy}\ Y^+_\alpha)\mathcal{H}_\alpha\begin{pmatrix} D_{\alpha,xy} \\ Y_\alpha \end{pmatrix},$$

$$H_Z = -\sum_{\alpha=1,2}(D^+_{\alpha,zx}\ Z^+_\alpha)\mathcal{H}_\alpha\begin{pmatrix} D_{\alpha,zx} \\ Z_\alpha \end{pmatrix},$$

$$\mathcal{H}_\alpha = E_0 + E_\alpha\begin{pmatrix} \cos\beta_\alpha & -\sin\beta_\alpha \\ -\sin\beta_\alpha & -\cos\beta_\alpha \end{pmatrix}, \tag{9}$$

with $E_0=(U-E_p)/2$, $E_\alpha=\sqrt{(U+E_p)^2/4+V_\alpha^2}$, and $V_{1,2}=V\sqrt{1\pm|\kappa|}$, $(\cos\beta_\alpha,\sin\beta_\alpha)=[(U+E_p)/2E_\alpha, V_\alpha/E_\alpha]$. H_Y and H_Z can be diagonalized through the rotation

$$\begin{pmatrix} D_{\alpha,xy} \\ Y_\alpha \end{pmatrix} = \begin{pmatrix} -\cos\beta_\alpha/2 & \sin\beta_\alpha/2 \\ \sin\beta_\alpha/2 & \cos\beta_\alpha/2 \end{pmatrix}\begin{pmatrix} \psi_\alpha \\ \varphi_\alpha \end{pmatrix},$$

$$\begin{pmatrix} D_{\alpha,zx} \\ Z_\alpha \end{pmatrix} = \begin{pmatrix} -\cos\beta_\alpha/2 & \sin\beta_\alpha/2 \\ \sin\beta_\alpha/2 & \cos\beta_\alpha/2 \end{pmatrix}\begin{pmatrix} \psi'_\alpha \\ \varphi'_\alpha \end{pmatrix} \tag{10}$$

into

$$H_Y = \sum_\alpha -(E_0+E_\alpha)\psi^+_\alpha\psi_\alpha + \sum_\alpha (E_\alpha - E_0)\varphi^+_\alpha\varphi_\alpha,$$

$$H_Z = \sum_\alpha -(E_0+E_\alpha)\psi'^+_\alpha\psi'_\alpha + \sum_\alpha (E_\alpha - E_0)\varphi'^+_\alpha\varphi'_\alpha. \tag{11}$$

Four degenerate levels $(\psi_1,\psi_2,\psi'_1,\psi'_2)$ are separated from the other four degenerate set $(\varphi_1,\varphi_2,\varphi'_1,\varphi'_2)$ with an energy spacing of nearly $U+E_p$. This large energy separation sets the stage for introducing spin-orbit interaction $H_{SO}=\lambda S\cdot L$ within each of the four-dimensional manifolds, but not between the two manifolds. We obtain the effective Hamiltonian valid within each manifold,

$$\mathcal{H} = \begin{pmatrix} \psi^+_1 \\ \psi^+_2 \\ \psi'^+_1 \\ \psi'^+_2 \end{pmatrix}^T\begin{pmatrix} -U_1 & 0 & -i\lambda_1 & -i\lambda_2 \\ 0 & -U_2 & -i\lambda_2 & -i\lambda_3 \\ i\lambda_1 & i\lambda_2 & -U_1 & 0 \\ i\lambda_2 & i\lambda_3 & 0 & -U_2 \end{pmatrix}\begin{pmatrix} \psi_1 \\ \psi_2 \\ \psi'_1 \\ \psi'_2 \end{pmatrix} + \begin{pmatrix} \varphi^+_1 \\ \varphi^+_2 \\ \varphi'^+_1 \\ \varphi'^+_2 \end{pmatrix}^T\begin{pmatrix} E^p_1 & 0 & -i\lambda'_1 & -i\lambda'_2 \\ 0 & E^p_2 & -i\lambda'_2 & -i\lambda'_3 \\ i\lambda'_1 & i\lambda'_2 & E^p_1 & 0 \\ i\lambda'_2 & i\lambda'_3 & 0 & E^p_2 \end{pmatrix}\begin{pmatrix} \varphi_1 \\ \varphi_2 \\ \varphi'_1 \\ \varphi'_2 \end{pmatrix}, \tag{12}$$

where $U_\alpha=E_0+E_\alpha$, $E^p_\alpha=E_\alpha-E_0$, and

$$i\lambda_1 = \langle\psi'_1|H_{SO}|\psi_1\rangle = \frac{i\lambda}{2}\cos^2\frac{\beta_1}{2}(m^x_r+m^x_l),$$

$$i\lambda_2 = \langle\psi'_1|H_{SO}|\psi_2\rangle = \langle\psi_2|H_{SO}|\psi'_1\rangle = \frac{i\lambda}{2}\cos\frac{\beta_1}{2}\cos\frac{\beta_2}{2}(m^x_r-m^x_l),$$

$$i\lambda_3 = \langle\psi'_2|H_{SO}|\psi_2\rangle = \frac{i\lambda}{2}\cos^2\frac{\beta_2}{2}(m^x_r+m^x_l),$$

$$i\lambda'_1 = \langle\varphi'_1|H_{SO}|\varphi_1\rangle = \frac{i\lambda}{2}\sin^2\frac{\beta_1}{2}(m^x_r+m^x_l),$$

$$i\lambda'_2 = \langle\varphi'_1|H_{SO}|\varphi_2\rangle = \langle\varphi_2|H_{SO}|\varphi'_1\rangle = \frac{i\lambda}{2}\sin\frac{\beta_1}{2}\sin\frac{\beta_2}{2}(m^x_r-m^x_l),$$

$$i\lambda'_3 = \langle\varphi'_2|H_{SO}|\varphi_2\rangle = \frac{i\lambda}{2}\sin^2\frac{\beta_2}{2}(m^x_r+m^x_l). \tag{13}$$

Here m^x_a refers to the x component of the local quantization axis for left and right magnetic sites. Because of small V/U, we can safely take

$$E_1 = E_2 = E = (U+E_p)/2,$$

$$\cos\beta_\alpha/2 \approx 1,$$

$$\sin\beta_\alpha/2 \approx V_\alpha/(U+E_p) \tag{14}$$

in Eq. (13). The above Hamiltonian $\mathcal{H}$ can be diagonalized to the form

$$\mathcal{H} = \sum_{i=1}^4 E^L_i\Psi^+_i\Psi_i + \sum_{i=1}^4 E^H_i\Phi^+_i\Phi_i, \tag{15}$$

with the eigenstates

$$\Psi_i = \xi^i_1\psi_1 + \xi^i_2\psi_2 + \xi^i_3\psi'_1 + \xi^i_4\psi'_2,$$

$$\Phi_i = \zeta^i_1\varphi_1 + \zeta^i_2\varphi_2 + \zeta^i_3\varphi'_1 + \zeta^i_4\varphi'_2. \tag{16}$$

One can verify that the coefficients satisfy

$$|\xi_1^i| = |\xi_3^i|, \quad |\xi_2^i| = |\xi_4^i|, \quad \bar{\xi}_1^i \xi_2^i = \bar{\xi}_3^i \xi_4^i \in \mathrm{Re},$$

$$|\zeta_1^i| = |\zeta_3^i|, \quad |\zeta_2^i| = |\zeta_4^i|, \quad \bar{\zeta}_1^i \zeta_2^i = \bar{\zeta}_3^i \zeta_4^i \in \mathrm{Re}. \tag{17}$$

This completes the formal derivation of the full set of eigenstates in the limit $U \gg \lambda, V$. The remaining task is to calculate the polarization $\langle \mathbf{r} \rangle$ for each of the eigenstates obtained.

Due to the shapes of d and p orbitals, only the following overlap integrals are nonzero ($\mathbf{x}=x\hat{x}$):

$$\langle d_{r,xy\sigma}|\mathbf{x}|p_{y\sigma}\rangle = \langle d_{l,xy\sigma}|\mathbf{x}|p_{y\sigma}\rangle = \langle d_{r,zx\sigma}|\mathbf{x}|p_{z\sigma}\rangle = \langle d_{l,zx\sigma}|\mathbf{x}|p_{z\sigma}\rangle = L\hat{x}. \tag{18}$$

Here $L=\int d^3\mathbf{r}\, d_{i,xy\sigma}(\mathbf{r})\mathbf{x}p_{y\sigma}(\mathbf{r})$ $(i=r,l)$. If nonzero polarization develops, it can only be in the $\hat{x}$ direction, i.e., along the axis of the three-atom cluster, within the lowest order in λ/Δ, $\Delta=U+E_p$. Note that the transverse component obtained in Ref. 10 corresponds to the terms of the first order in λ/Δ. This contribution is numerically studied later in Sec. III. The final expression for the polarization $\mathbf{P}$ reads (details are given in the Appendix)

$$\mathbf{P}_{\Psi_i} = \langle \Psi_i|\mathbf{r}|\Psi_i\rangle = 2\bar{\xi}_1^i \xi_2^i [\langle \psi_1|\mathbf{r}|\psi_2\rangle + \langle \psi_1'|\mathbf{r}|\psi_2'\rangle] \approx \hat{x}\frac{8\bar{\xi}_1^i \xi_2^i LV}{\Delta},$$

$$\mathbf{P}_{\Phi_i} = \langle \Phi_i|\mathbf{r}|\Phi_i\rangle = \frac{1}{2}\bar{\zeta}_1^i \zeta_2^i [\langle \varphi_1|\mathbf{r}|\varphi_2\rangle + \langle \varphi_1'|\mathbf{r}|\varphi_2'\rangle] \approx -\hat{x}\frac{\sqrt{2}\bar{\zeta}_1^i \zeta_2^i LV}{\Delta}\sqrt{1-\sigma_1\cdot\sigma_2}. \tag{19}$$

Note that $\bar{\xi}_1^i \xi_2^i$ and $\bar{\zeta}_1^i \zeta_2^i$ are also dependent on the spin configuration. The full spin dependence of the polarization may be rather complicated. However, because of small V/U, we can take $U_1=U_2=U$ and

$$\lambda_1 = \lambda_3 = \frac{\lambda}{2}(m_l^x + m_r^x),$$

$$\lambda_2 = \frac{\lambda}{2}(m_r^x - m_l^x). \tag{20}$$

Under such an approximation the low-energy eigenstates are given by the surprisingly simple form

$$\Psi_1 = (i\psi_1 + i\psi_2 + \psi_1' + \psi_2')/2, \quad E_1^L = -U - \lambda_1 - \lambda_2,$$

$$\Psi_2 = (i\psi_1 - i\psi_2 - \psi_1' + \psi_2')/2, \quad E_2^L = -U + \lambda_1 - \lambda_2,$$

$$\Psi_3 = (-i\psi_1 + i\psi_2 - \psi_1' + \psi_2')/2, \quad E_3^L = -U - \lambda_1 + \lambda_2,$$

$$\Psi_4 = (-i\psi_1 - i\psi_2 + \psi_1' + \psi_2')/2, \quad E_4^L = -U + \lambda_1 + \lambda_2. \tag{21}$$

For each of the eigenstates above, the polarization $\mathbf{P}_{\Psi_i}$ reads

$$\mathbf{P}_{\Psi_1} = \mathbf{P}_{\Psi_4} = \hat{x}\frac{2LV}{\Delta},$$

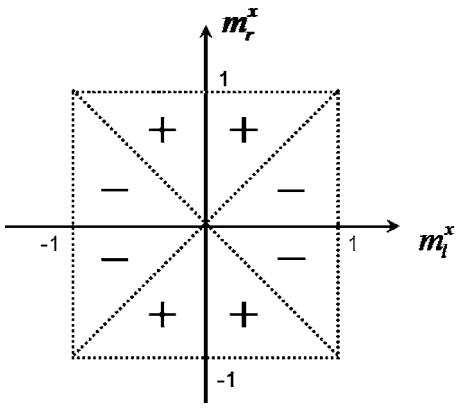

FIG. 2. The direction of longitudinal polarization $P_x=\mathbf{P}\cdot\hat{x}$ in the ground state wave function plotted for (m_l^x, m_r^x), $-1 \leqslant m_l^x, m_r^x \leqslant 1$. $+(-)$ refers to $P_x > (<) 0$. P_x is indeterminate along two dotted lines ($m_r^x = m_l^x$ and $m_r^x = -m_l^x$) due to the level crossing occuring along these lines.

$$\mathbf{P}_{\Psi_2} = \mathbf{P}_{\Psi_3} = -\hat{x}\frac{2LV}{\Delta}. \tag{22}$$

The polarization, constant in magnitude but reversible in sign, is developed along the M-O-M cluster. Since λ_1 and λ_2 depend on the spin directions and in particular on m_l^x and m_r^x as shown in Eq. (20), which one of the four states shown in Eq. (21) becomes the true ground state depends on the set of values (m_l^x, m_r^x). In Fig. 2 we map out the polarization directions of the ground state for all the available situations within the zeroth order in λ/Δ. The reversal of the polarization direction occurs whenever the $|m_l^x| = |m_r^x|$ line is crossed. The sudden change of the sign is due to the level crossing of the two eigenstates when λ_1 or λ_2 vanishes at $|m_l^x| = |m_r^x|$. The ground state polarization is consistent with the functional form $P_x \sim (m_r^x)^2 - (m_l^x)^2$.

If a single hole is introduced in the cluster, the polarization is given by one of the expressions in Eq. (22). With two holes, two opposite polarizations from Eq. (22) cancel out to produce $\mathbf{P}=0$. In the numerical results presented in the next section, however, one finds a finite longitudinal polarization even for the two-hole case because of the higher-order terms in λ/Δ, and the polarization direction is still dictated by $P_x \sim (m_r^x)^2 - (m_l^x)^2$.

III. NUMERICAL RESULTS

The results of the previous section gave the electronic polarization solely along the axis of the atomic cluster. In the analysis it was assumed that the large effective Zeeman energy U dominates over both the spin-orbit interaction λ and the hybridization amplitude V. It was also assumed that d_{yz} and p_x orbitals did not play a role. According to Ref. 10, on the other hand, transverse polarization such as P_y can only arise from the overlap integral $\langle d_{yz}|y|p_z\rangle$ or $\langle d_{xy}|y|p_x\rangle$. In the numerical approach, this condition can be relaxed and indeed we find nonzero transverse polarization as well as the longitudinal polarization in accordance with the theory presented in the previous section. In general, the results depend sensi-

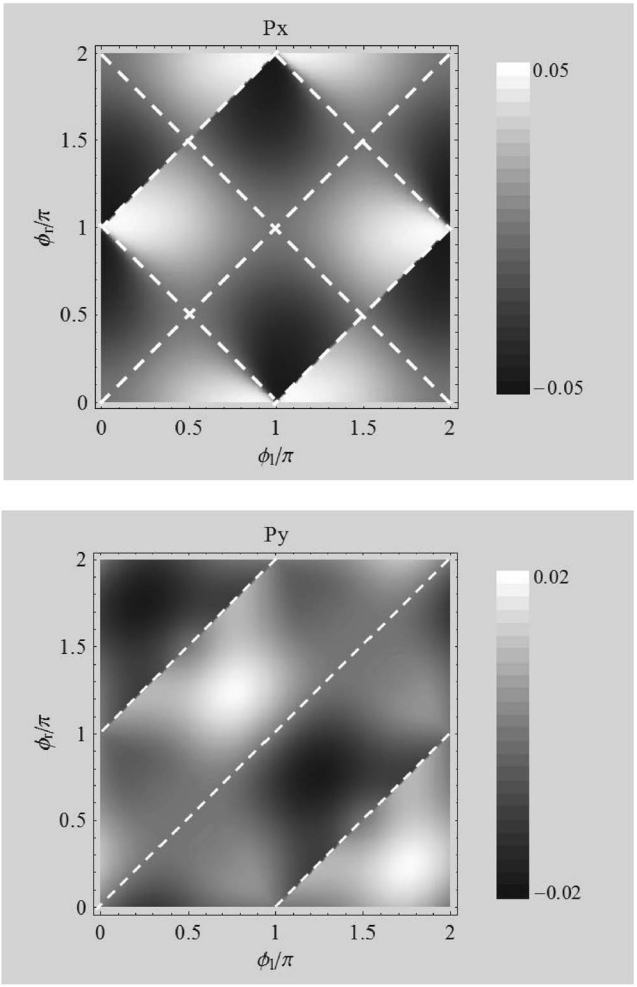

FIG. 3. The calculated polarization P_x and P_y from exact diagonalization of the full M-O-M cluster Hamiltonian with a single hole. Dotted white lines indicate P_x or P_y equal to zero. P_x vanishes not only when the spins are collinear, but also when $\phi_l+\phi_r=\pm\pi$, as discussed in Sec. II. The overall directional dependence for P_x is consistent with $\cos 2\phi_r-\cos 2\phi_l$. The sharp change in the sign of P_x along $\phi_r=\phi_l\pm\pi$ lines is due to the energy level crossing in the ground state. P_y turns to zero along the lines (indicated as dotted white lines) where the spins become collinear. The parameters used in this calculation are $(U/V, E_p/V, \lambda/V)=(10, 30, 0.3)$.

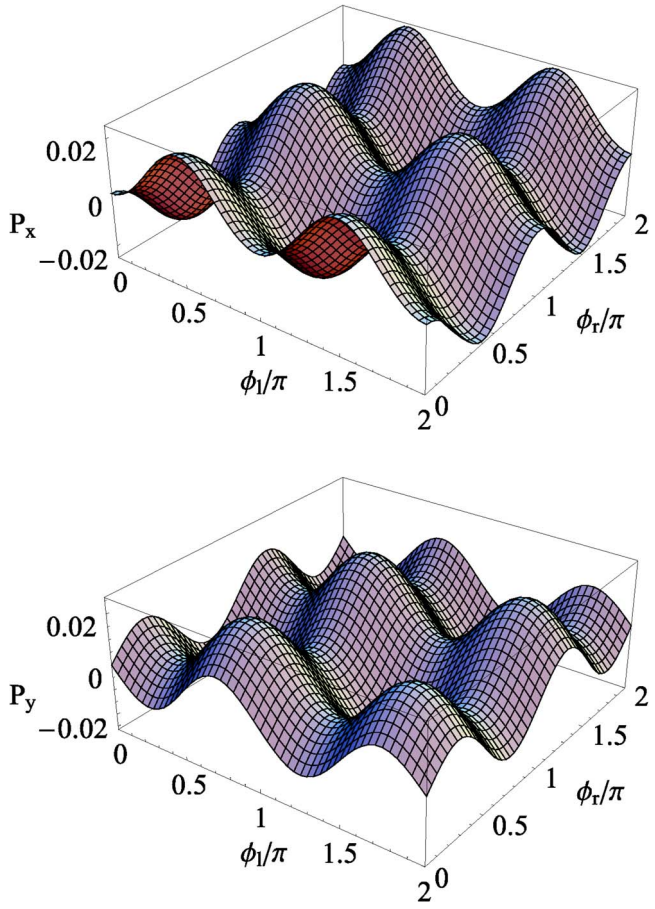

FIG. 4. (Color online) Induced polarization P_x and P_y in a unit of L for the superexchange case with two holes in the three-atom cluster. The parameters used in this calculation are the same as in Fig. 3.

tively on the number of holes inserted in the cluster, with the even and odd number of holes yielding different behavior. As a representative case for each, we consider one- and two-hole situations in detail. When extrapolated to the infinite lattice they correspond to the metallic and insulating cases, respectively.

The Hilbert space for the single-particle mean-field Hamiltonian is 18-dimensional, consisting of Eq. (1) and Eq. (2), with six from each atomic site. In practice, one can treat the 16-dimensional problem leaving out the oxygen p_x orbital without loss of generality, since it remains decoupled from the rest of the atomic states in the exact solution.

A. One hole (double-exchange interaction)

The polarization $\langle \mathbf{r} \rangle$ is calculated with respect to the lowest-energy eigenstate of the particle-hole transformed Hamiltonian corresponding to putting one hole in the cluster. For ease of presentation we restrict ourselves to situations where both spins lie in the XY plane: $\hat{m}_l=(\cos\phi_l, \sin\phi_l, 0)$, and $\hat{m}_r=(\cos\phi_r, \sin\phi_r, 0)$. The resulting longitudinal polarization P_x is plotted as a function of (ϕ_l, ϕ_r) in Fig. 3. The similarity between the numerically obtained P_x and the predicted behavior $P_x \sim \cos 2\phi_r - \cos 2\phi_l$ is striking. The magnitude of the polarization, according to Eq. (22) and using the parameters used in the numerical study, is expected to be $|P_x| \sim 0.05L$, in good agreement with the numerical results.

In addition, we find nonzero P_y in the numerical calculation due to the inclusion of the d_{yz} orbital. The behavior of P_y we find is consistent with the directional dependence $P_y \sim \mathrm{sgn}[\cos(\Delta\phi/2)]\sin(\Delta\phi/2)(\Delta\phi=\phi_r-\phi_l)$ expected in Ref. 10 [see Eq. (4) in Ref. 10]. Also the order of magnitude $|P_y| \sim 0.01L$ obtained numerically is consistent with Ref. 10. P_z vanishes for the two spins lying in the XY plane, as shown both analytically and numerically.

B. Two holes (superexchange interaction)

When two holes are introduced in the cluster, the ground state can be changed adiabatically without a level crossing as the two spin directions are varied, and hence the polarization

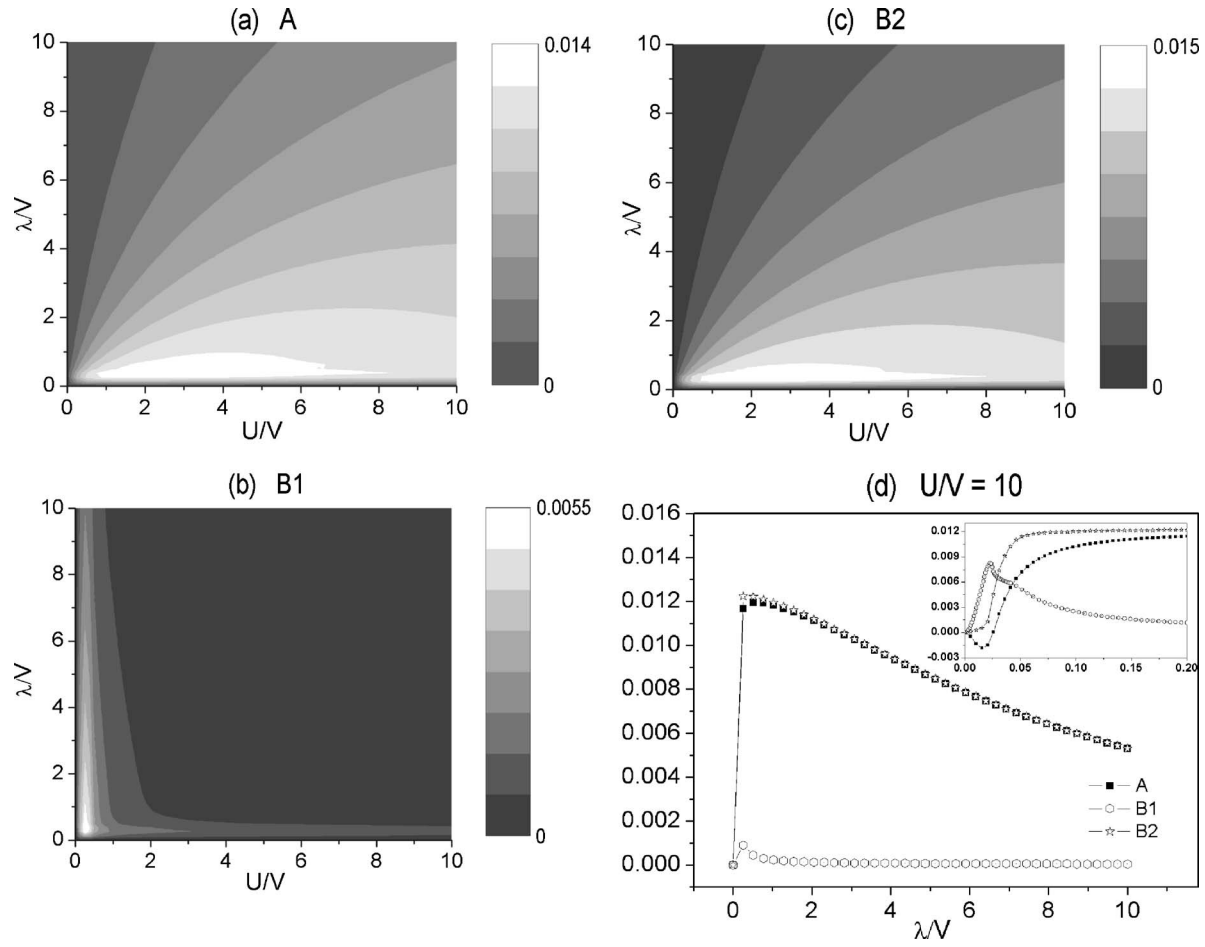

FIG. 5. (a)–(c) Fourier components A, B_1, and B_2 in the polarization P_x/L and P_y/L using the fitting formula, Eq. (23). (d) Fourier components with $U/V=10$ and varying λ/V. The inset shows very small λ/V results.

exhibits a smooth change. Typical numerical results for the longitudinal and transverse components of the polarization are shown in the upper and lower panels of Fig. 4. As in the previous consideration for one hole, the spin directions are varied within the XY plane with $\hat{m}_l=(\cos\phi_l,\sin\phi_l,0)$ and $\hat{m}_r=(\cos\phi_r,\sin\phi_r,0)$.

We analyzed the directional dependence of the polarization by using the following forms:

$$P_x/L = A[\cos(2\phi_r) - \cos(2\phi_l)],$$

$$P_y/L = -B_1\sin(\phi_r - \phi_l) + B_2[\sin(2\phi_r) - \sin(2\phi_l)]. \tag{23}$$

While the least-square fit to the numerical results were made using as many as six different basis functions, only those listed above made a sizable contribution. The angle dependence of the transverse polarization P_y predicted in Ref. 10 corresponds to the $B_1\sin(\phi_r-\phi_l)$ term above, whereas the angle dependence of P_x is consistent with the single-hole results analytically derived in the previous section. The second term in P_y, proportional to B_2, was not anticipated in analytic theories but did show up in the numerical analysis. In the spiral phase for the spins, $B_1\sin(\phi_r-\phi_l)$ produces a uniform transverse component while all other terms give rise to a macroscopically vanishing polarization. In this regard the terms (A and B_2) correspond to the "oscillating" component of the polarization in contrast to the uniform component given by B_1.

Figure 5 shows the coefficients, A, B_1, and B_2, for a wide range of parameters, $0\leqslant\lambda/V\leqslant 10$, $0\leqslant U/V\leqslant 10$, obtained by fitting the numerical data using Eq. (23). Several features are worth mentioning. (i) A and B_2 are remarkably similar over most of the parameter space. This implies that the nonuniform polarization develops with similar magnitudes along and orthogonal to the bond axis. (ii) Large nonuniform polarization components are attained for large U/V and small λ/V. On the other hand, large uniform polarization (B_1) is achieved for large λ/V and small U/V in agreement with Ref. 10, where $\lambda\gtrsim U$ was implicitly assumed. To be concrete, the largest values for A, B_1, and B_2 are obtained for $(U/V,\lambda/V)=(1.795,0.256)$, (0.256, 0.256), and (1.794, 0.256), respectively, with the magnitudes indicated on the vertical bar next to each figure. Using an earlier estimate,[10] these maximal values correspond to $A\sim B_2\sim 2\times 10^2$ nC/cm^2 and $B_1\sim 80$ nC/cm^2. For U/V large, the polarization mainly possesses the oscillating components with a much smaller uniform component as explicitly demonstrated at the bottom of Fig. 5 for U/V fixed at a large value ($U/V=10$) and varying λ/V.

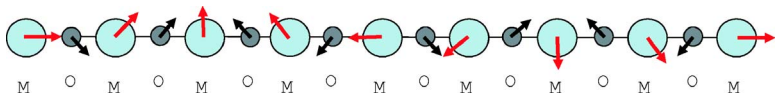

FIG. 6. (Color online) Spiral spin structure (red arrows) with an angle shift of $\pi/4$ between neighboring magnetic (M) ions and the induced dipole moments (parallel or antiparallel to black arrows) at oxygen (O) sites with half the periodicity. The uniform component is not shown since it is much smaller than the nonuniform part.

The macroscopic polarization is governed by the B_1 term alone. On the other hand, the Fourier analysis reveals the local magnitudes of the oscillating component to be much larger than the uniform polarization over most of the parameter ranges, increasing the chance to observe coupling of the local dipole order to external probes such as x-ray or neutron scattering. Particularly in spiral magnets with ordering wave vector $\boldsymbol{Q}$, the oscillation of electric dipole moments appears with the wave vector $2\boldsymbol{Q}$, since we have found that the nonuniform part has the form $\sin 2\phi_l - \sin 2\phi_r$ for the transverse component and $\cos 2\phi_l - \cos 2\phi_r$ for the longitudinal one. Figure 6 shows the simplest example with the periodicity of the eight M ions where relative angles between the neighboring spins are $\pi/4$. In this case, electric dipole moments induced at oxyen ions also helically rotate with half the magnetic periodicity. Note that the amplitude of this nonuniform part is much larger than the uniform part. It is expected that oxygen ions subject to such electric dipole field shift in either parallel or antiparallel directions to the local dipole moment.

IV. DISCUSSION

In this paper we have developed a theory for the spin-induced electric polarization in a simple three-atom cluster model proposed in Ref. 10. The truncation to the low-energy space is allowed by the large energy separation between spin-up and spin-down states of the magnetic site due to the strong effective Zeeman field, and the much smaller energy scale for the *pd*-hybridization V and spin-orbit interaction λ. The net electric dipole moment is found to be along the cluster's axis within our approximation, and the numerical calculation confirmed this conclusion. The longitudinal polarization has an oscillating character and vanishes in the macroscopic limit. Numerical analysis further identified uniform and nonuniform components in the transverse polarization. The magnitude of the nonuniform transverse polarization is comparable to the nonuniform longitudinal one. Such nonuniform polarizations generically have larger magnitudes on the atomic scale than the uniform transverse component.

In this paper we have concentrated on the t_{2g} electron systems because the spin-orbit interaction has the matrix elements within the t_{2g} orbitals, while they are zero among the e_g orbitals. The effective Zeeman field at each site corresponds to the mean field from the surrounding spins, which leads to a model similar to the double exchange model discussed in this paper. Generalizations to the more realistic models including the hybridization between e_g and t_{2g} orbitals and spin-orbit interaction on oxygen orbitals are now in progress, which will be applied to realistic materials such as $R\mathrm{MnO}_3$ (R=Tb,Gd). However, our present model will have relevance to materials such as YVO_3 (Ref. 12) or $R_2\mathrm{Ti}_2\mathrm{O}_7$ (R=Gd,Tb),[13] which have partially filled t_{2g} electrons. More serious considerations on each material including the finite bond angle, etc. are left for future investigations.

Recent experimental works on multiferroics with spiral spin structure with the ordering wave vector $\boldsymbol{Q}$ have reported the lattice modulation at the wave vector $2\boldsymbol{Q}$ in addition to the macroscopic polarization.[1] Since dipole moments are linearly coupled to the ionic displacements, it may correspond to the nonuniform dipole moments shown in this paper. In our scenario of magnetically induced dipole moments, the modulation of the oxygen ions is noncollinear and also has a spiral structure, reminiscent of the MnSi case.[14] A similar lattice modulation but with the collinear shifts has been discussed by Sergienko and Dagotto.[11] Further x-ray and neutron scattering experiments are required to specify the detailed character of this lattice modulation.

On the theory side, a Ginzburg-Landau consideration led to the conclusion that the uniform polarization direction is orthogonal to the modulation wave vector of the spin.[8,9] In Ref. 8 some nonuniform components of the polarization are predicted on the basis of Ginzburg–Landau theory without a detailed discussion of its implications. Furthermore, consideration of the orbital structure for the magnetic site is missing in the phenomenological theories advanced so far. For instance, the t_{2g} levels alone break the rotational symmetry in the orbital space and the corresponding Ginzburg–Landau theory need not possess the invariance under spatial rotation. It will be interesting to develop a Ginzburg–Landau theory with a proper symmetry consideration for the t_{2g} systems to see if the features we observe, i.e., nonuniform longitudinal and transverse polarizations, emerge naturally.

ACKNOWLEDGMENTS

The authors thank T. Arima for fruitful discussions. This work was partly supported by Sungkyunkwan University (C.J.), Grants-in-Aid (Grant No. 15104006, No. 16076205, and No. 17105002) and NAREGI Nanoscience Project from the Ministry of Education, Culture, Sports, Science, and Technology, Japan.

APPENDIX: CALCULATION OF THE DIPOLE MOMENTS

In this appendix, we give details of analytic calculations of dipole moments associated with the approximate eigenstates of the total Hamiltonian.

1. Diagonal terms

Since

$$\langle Y_1|\mathbf{r}|D_{1,xy}\rangle = \frac{L}{2\sqrt{1+|\kappa|}}[1-1+|\kappa|-|\kappa|]\hat{x} = 0, \quad \text{(A1)}$$

we have

$$\langle \psi_1|\mathbf{r}|\psi_1\rangle = -\frac{\sin\beta_1}{2}[\langle D_{1,xy}|\mathbf{r}|Y_1\rangle + \langle Y_1|\mathbf{r}|D_{1,xy}\rangle] = 0,$$

$$\langle \varphi_1|\mathbf{r}|\varphi_1\rangle = \frac{\sin\beta_1}{2}[\langle D_{1,xy}|\mathbf{r}|Y_1\rangle + \langle Y_1|\mathbf{r}|D_{1,xy}\rangle] = 0. \tag{A2}$$

All other diagonal terms vanish as well: $\langle \psi_m|\mathbf{r}|\psi_m\rangle = \langle \psi'_m|\mathbf{r}|\psi'_m\rangle = \langle \varphi_m|\mathbf{r}|\varphi_m\rangle = \langle \varphi'_m|\mathbf{r}|\varphi'_m\rangle = 0$.

2. Off-diagonal terms

In view of the symmetry of the orbital overlaps given in Eq. (18), the following averages must be zero: $\langle \psi_1|\mathbf{r}|\psi'_1\rangle = \langle \psi_1|\mathbf{r}|\psi'_2\rangle = \langle \psi_2|\mathbf{r}|\psi'_1\rangle = \langle \psi_2|\mathbf{r}|\psi'_2\rangle = 0$.

3. Dipole moments for the eigenstates

Thus only $\langle \psi_1|\mathbf{r}|\psi_2\rangle$, $\langle \psi'_1|\mathbf{r}|\psi'_2\rangle$ and $\langle \varphi_1|\mathbf{r}|\varphi_2\rangle$, $\langle \varphi'_1|\mathbf{r}|\varphi'_2\rangle$ may contribute to the polarization. Since

$$\langle D_{1,xy}|\mathbf{r}|Y_2\rangle = -\hat{x}L\sqrt{1-|\kappa|},$$

$$\langle Y_1|\mathbf{r}|D_{2,xy}\rangle = -\hat{x}L\sqrt{1+|\kappa|}, \tag{A3}$$

we have

$$\begin{aligned}\langle \psi_1|\mathbf{r}|\psi_2\rangle &= -\cos\frac{\beta_1}{2}\sin\frac{\beta_2}{2}\langle D_{1,xy}|\mathbf{r}|Y_2\rangle \\ &\quad - \sin\frac{\beta_1}{2}\cos\frac{\beta_2}{2}\langle Y_1|\mathbf{r}|D_{2,xy}\rangle \\ &\simeq \hat{x}\frac{LV}{\Delta}[(1-|\kappa|)+(1+|\kappa|)] \\ &= \hat{x}\frac{2LV}{\Delta},\end{aligned}$$

$$\begin{aligned}\langle \varphi_1|\mathbf{r}|\varphi_2\rangle &= \sin\frac{\beta_1}{2}\cos\frac{\beta_2}{2}\langle D_{1,xy}|\mathbf{r}|Y_2\rangle \\ &\quad + \cos\frac{\beta_1}{2}\sin\frac{\beta_2}{2}\langle Y_1|\mathbf{r}|D_{2,xy}\rangle \\ &\simeq -\hat{x}\frac{2LV}{\Delta}\sqrt{1-|\kappa|^2} \\ &= -\hat{x}\times\frac{\sqrt{2}LV}{\Delta}\sqrt{1-\sigma_1\cdot\sigma_2}.\end{aligned} \tag{A4}$$

Similarly,

$$\langle D_{1,zx}|\mathbf{r}|Z_2\rangle = -\hat{x}L\sqrt{1-|\kappa|},$$

$$\langle Z_1|\mathbf{r}|D_{2,zx}\rangle = -\hat{x}L\sqrt{1+|\kappa|} \tag{A5}$$

gives

$$\begin{aligned}\langle \psi'_1|\mathbf{r}|\psi'_2\rangle &= -\cos\frac{\beta_1}{2}\sin\frac{\beta_2}{2}\langle D_{1,zx}|\mathbf{r}|Z_2\rangle \\ &\quad - \sin\frac{\beta_1}{2}\cos\frac{\beta_2}{2}\langle Z_1|\mathbf{r}|D_{2,zx}\rangle \\ &\simeq \hat{x}\frac{2LV}{\Delta},\end{aligned}$$

$$\begin{aligned}\langle \varphi'_1|\mathbf{r}|\varphi'_2\rangle &= \sin\frac{\beta_1}{2}\cos\frac{\beta_2}{2}\langle D_{1,zx}|\mathbf{r}|Z_2\rangle \\ &\quad + \cos\frac{\beta_1}{2}\sin\frac{\beta_2}{2}\langle Z_1|\mathbf{r}|D_{2,zx}\rangle \\ &\simeq -\hat{x}\frac{\sqrt{2}LV}{\Delta}\sqrt{1-\sigma_1\cdot\sigma_2}.\end{aligned} \tag{A6}$$

*Author to whom correspondence should be addressed. Electronic address: hanjh@skku.edu

[1] T. Kimura, T. Goto, H. Shintani, K. Ishizaka, T. Arima, and Y. Tokura, Nature (London) **426**, 55 (2003).
[2] N. Hur, S. Park, P. A. Sharma, J. S. Ahn, S. Guha, and S.-W. Cheong, Nature (London) **429**, 392 (2004).
[3] G. Lawes, A. B. Harris, T. Kimura, N. Rogado, R. J. Cava, A. Aharony, O. Entin-Wohlman, T. Yildrim, M. Kenzelmann, C. Broholm, and A. P. Ramirez, Phys. Rev. Lett. **95**, 087205 (2005).
[4] M. Kenzelmann, A. B. Harris, S. Jonas, C. Broholm, J. Schefer, S. B. Kim, C. L. Zhang, S.-W. Cheong, O. P. Vajk, and J. W. Lynn, Phys. Rev. Lett. **95**, 087206 (2005).
[5] T. Arima, T. Goto, Y. Yamasaki, S. Miyasaka, K. Ishii, M. Tsubota, T. Inami, Y. Murakami, and Y. Tokura, Phys. Rev. B **72**, 100102(R) (2005).
[6] T. Arima, A. Tokunaga, T. Goto, H. Kimura, Y. Noda, and Y. Tokura, Phys. Rev. Lett. **96**, 097202 (2006).
[7] Y. Yamasaki, S. Miyasaka, Y. Kaneko, J.-P. He, T. Arima, and Y. Tokura, Phys. Rev. Lett. **96**, 207204 (2006).
[8] Maxim Mostovoy, Phys. Rev. Lett. **96**, 067601 (2006).
[9] A. B. Harris and G. Lawes, cond-mat/0508617 (unpublished); A. B. Harris, cond-mat/0508730 (unpublished); A. B. Harris, T. Yildirim, A. Aharony, and O. Entin-Wohlman, cond-mat/0510807 (unpublished).
[10] Hosho Katsura, Naoto Nagaosa, and Alexander V. Balatsky, Phys. Rev. Lett. **95**, 057205 (2005).
[11] I. A. Sergienko and E. Dagotto, Phys. Rev. B **73**, 094434 (2006).
[12] Y. Ren, T. T. M. Palstra, D. I. Khomskii, E. Pellegrin, A. A. Nugroho, A. A. Menovsky, and G. A. Sawatsky, Nature (London) **396**, 441 (1998).
[13] M. J. Harris, S. T. Bramwell, D. F. McMorrow, T. Zeiske, and K. W. Godfrey, Phys. Rev. Lett. **79**, 2554 (1997).
[14] M. L. Plummer and M. B. Walker, J. Phys. C **15**, 7181 (1982).